Aggregation of Syndiotactic Poly(methyl methacrylate) in Dilute Solutions

Blahoslav Sedláček,* Jiří Spěváček, Libuše Mrkvičková, Jaroslav Stejskal, Jitka Horská, Josef Baldrian, and Otto Quadrat

Institute of Macromolecular Chemistry, Czechoslovak Academy of Sciences, 162 06 Prague 616, Czechoslovakia. *Received August 1, 1983*

ABSTRACT: A combination of several methods and quantitative parameters (fraction p of immobilized monomer units, apparent molecular weight, and size, number, and concentration of aggregates) as a function of time, temperature, and polymer concentration were used to obtain data characterizing aggregation of syndiotactic poly(methyl methacrylate) in *n*-butyl acetate. The thermal history of the sample (viz., the content of surviving nuclei which were identified with aggregates of globules formed during the intramolecular condensation) was shown to be decisive for the setting in and steepness of the aggregation process. Another "hysteretic" effect has been found by NMR for the equilibrium value of p at elevated temperatures. Regarding all experimental and reported data, a plausible qualitative model of aggregation was suggested; three processes, "globulation", nucleation, and flocculation, were recognized and characterized.

I. Introduction

The solution behavior of isotactic (i), syndiotactic (s), and atactic (a) poly(methyl methacrylate) has been studied extensively for many years.[1–19] Several methods, viz., NMR and IR spectroscopy, Rayleigh–Gans–Debye (R–G–D) light scattering, gel permeation chromatography (GPC), viscometry, osmometry, and wide-angle X-ray scattering (WAXS), have been used for this purpose. Association and aggregation of either isotactic or syndiotactic PMMA's (and even a-PMMA[14]) or their mixtures[10–12,15,16] were observed both in dilute solutions and in bulk. In dilute solutions, stereocomplex (i,s)-PMMA and its individual stereoforms were recognized to be responsible for the ordering process leading to a local intramolecular "crystallization" or to an interparticle stereoassociation (aggregation).[15h] The influence of solvent specificity, polymer concentration, aggregation temperature, and degree of stereoregularity was shown to be decisive for the character of such processes, viz., of their course and products. The crystalline content found in bulk seems to be closely connected with the solvent-induced crystallization.[13c,16i] Strongly complexing, weakly complexing, and noncomplexing solvents may be classified as to their PMMA crystallite forming ability.[15d]

In spite of a great number of papers containing a remarkable quantity of information about mutual and polymer–solvent interactions of the stereoregular forms of PMMA, the problem still remains far from being understood completely. The reason for this is the considerable complexity of the processes occurring in such interacting systems and the need to deal with particles of a size ranging from molecular to colloidal. In recent years, increasing attention has been paid to polymer colloids,[20–31] particularly to "ideal" systems suitable for testing theories. Therefore, for a flocculating "real" system, the same degree of fitting between model predictions and experimental findings can be hardly expected.

The aim of this paper is to formulate, on the basis of consistent experimental results and considerations, a plausible qualitative model of changes occurring within the whole aggregation process of s-PMMA in *n*-butyl acetate, from the growth initiation up to the precipitation of particles. For this purpose, experimental data characterizing quantitative parameters of particles in aggregating systems (viz., fraction of immobilized monomer units, apparent molecular weight, and size, number, and concentration of aggregates) have been obtained by using nearly all the techniques mentioned above (supplemented by two Lorenz–Mie light scattering methods). Some apparent discrepancies between results supplied by individual methods are satisfactorily explained by their different relationship to the effect investigated.

II. Methods and Procedures

Samples. Syndiotactic poly(methyl methacrylate) (s-PMMA) was prepared in toluene solution by coordination polymerization catalyzed by titanium(IV) chloride and triethylaluminum at −78 °C. The s-PMMA samples were unimodal in molecular weight distribution; their characteristics are given in Table I. The purity of *n*-butyl acetate (BAC) and toluene was checked by gas chromatography (content of impurities ~0.1%).

Wide-Angle X-ray Scattering (WAXS). Individual samples of s-PMMA-1 and s-PMMA-2 dissolved in BAC and acetone were cooled to 25 °C; the suspension was isolated by centrifugation and evaporation of the respective solvent at the same temperature. "Dry" samples (containing ~5% solvent) were measured by WAXS using a Hilger and Watts powder diffractometer; the Cu Kα radiation was monochromatized with a Ni filter. Registration was carried out with a scintillation counter; an amplitude analyzer was also used.

NMR Spectroscopy. Solutions of s-PMMA-1 in BAC and toluene-d_8 ($c_0 = 9.0 \times 10^{-3}$ g cm^{-3}) were prepared directly in NMR tubes (which were then sealed) and homogenized in a bath at 100 °C for 48 h. Before the ^{1}H NMR spectra were recorded, the solutions were thermostated at 80 °C for 30 min and placed in the spectrometer probe, which was preheated to the desired temperature: a further 3–4 min was needed for thermal equilibration, after which (time $t = 0$) the time dependence could be measured. A JEOL PS-100 spectrometer was used for observation of the ^{1}H NMR spectra at 100 MHz.

Viscometry. The viscosity was measured in capillary viscometers of the Ostwald type with closed circulation to eliminate solvent evaporation. The flow time of solvent was about 100 s. Corrections for non-Newtonian effects and loss in kinetic energy were negligible. The viscometer was tested for accurate measurement of highly aggregated samples (using capillaries with two different diameters): no interference of aggregates with the viscometer capillary was observed. At the beginning of each experiment, the solutions were heated in the viscometer for 20 min above the dissolution temperature of aggregates, i.e., to 85 °C in BAC and 60 °C in toluene, as estimated from earlier viscometric measurements. The system then was cooled to 40–53 °C (BAC) or 25–40 °C (toluene) and flow times were measured at appropriate intervals. The chosen temperature intervals (and the polymer concentration, $c_0 = 9.0 \times 10^{-3}$ g cm^{-3} maximum) were the best suited: at lower aggregation temperatures, the viscosity change would be too fast while at higher temperatures it would be too slow.

Osmometry. Osmotic pressure of s-PMMA-2 in BAC at 60 °C was measured with an automatic Knauer membrane osmometer. Samples were dissolved in ampules (sealed after filling) at 100 °C within a few hours. During the osmotic measurements, the samples were kept at 60 °C, where the aggregation process was so slow that, for obtaining data over the whole concentration scale, no isochronous treatment was needed. Individual con-

0024-9297/84/2217-0825$01.50/0

Table I
Characteristics of Syndiotactic Poly(methyl methacrylate) Samples[a]

sample	$10^{-5}M_w$	M_w/M_n	$\bar{l}_s$*	content of triads, %		
				syndiotactic	heterotactic	isotactic
s-PMMA-1	5.5	1.3	25.4	91.5	7.5	1
s-PMMA-2	2.6	1.4	22.1	89.5	8.5	2

[a] M_w measured by light scattering in chloroform at 25 °C; M_w/M_n from GPC measurements in tetrahydrofuran at 25 °C; stereoregularity by ^{1}H NMR spectroscopy in an equimolar mixture of *o*-dichlorobenzene and tetrachloroethylene at 140 °C; $\bar{l}_s^* = (2s + h)/h$ is the mean syndiotactic sequence length.

Table II
Aggregation Experiments: Treatment of Samples and Turbidity Characteristics[a]

expt series	history		treated (min)		aggregation time t (min) at τ						
	°C	min	at DT	at AT	0.7	Δ	1.4	Δ	2.8	Δ	4.2
Series A (DT = 70 °C; AT = 52 °C)											
A1/1*	100	d[b]	15	140	73.0	14.5	87.5	20.0	107.5	18.5	126.0
A1/2*	52	140	15[d]	128[d]	45.5	11.5	57.0	7.5	74.5	24.0	98.5
A2/1	100	d[b]	15	186	93.0	14.0	107.0	63.0	170.0		
Series B (DT = 70 °C; AT = 50 °C)											
B1/1*	80	d	20	66	35.5	7.0	42.5	9.0	51.5	7.2	58.7
B1/2*	50	66	20[e]	60	28.0	7.0	35.0	8.0	43.0	10.0	53.0
B1/3*	50	60	20[e]	60	27.0	7.5	32.5	8.5	41.0	10.5	51.5
B1/4*	50	60	20[e]	60	27.0	6.3	33.3	8.7	42.0	11.5	53.5
B2/1	52	186	15[d]	150	42.5	10.5	53.0	14.5	77.5		
B3/1	80	d	15[e]	56	33.6	5.7	39.3	7.2	46.5	6.1	52.6
B3/2	50	56	30	43	16.3	4.0	20.3	6.2	26.5	10.0	36.5
Series C (DT = 80 °C; AT = 50 °C)											
C1/1	50	50	30[e]	63	38.3	3.9	44.2	7.8	52.0	6.7	58.7
C1/2	50	63	30[e]	65	39.4	6.2	45.6	7.7	53.3	6.9	60.2
Series D (DT = 70 °C; AT = 48 °C)											
D1/1	80	d	20	72	49.5	8.5	58.0	12.0	70.0		
D1/2	48	72	20[d]	60	35.0	7.5	42.5	10.0	52.5		
D1/3	48	60	20[d]	60	34.0	7.5	41.5	13.0	54.5		
D1/4	48	60	20[d]	60	32.0	6.5	38.5	15.0	53.5		
D2/1	48	36	30[c]	33	20.5	3.0	23.5	3.9	27.4	3.7	31.1
D2/2	48	33	30	30	12.3	2.1	14.4	3.7	18.1	5.2	23.3
D3/1	80	d	15	37	22.7	3.3	26.0	4.1	30.1	3.5	33.6
D3/2	48	37	30	29	11.8	2.5	14.3	3.8	18.1	5.5	23.6
D3/3	48	29	30	31	11.1	2.6	13.7	4.2	17.9	7.0	24.9
Series E (DT = 80 °C; AT = 48 °C)											
E1/1	25	d	30	34	19.4	2.8	22.2	3.9	26.1	3.1	29.2
E1/2	48	34	30	37	23.6	3.8	27.4	3.4	30.8	3.7	34.5
E1/3	48	37	30	38	25.2	3.4	28.6	4.3	32.9	3.7	36.6
E1/4	48	38	30	39	24.8	3.4	28.2	4.2	32.4	3.7	36.1
E1/5	48	39	30	36	25.1	3.3	28.4	4.3	32.7	3.7	36.4

[a] Samples (with history) were treated at dissolution (DT) and aggregation (AT) temperatures. Turbidity curves are characterized by "isoturbs" (time needed to reach the given turbidity) and their differences Δ (inversely proportional to their steepness). Concentration $c_0 = 4.5 \times 10^{-3}$ and 9.0×10^{-3} g cm^{-3} (the latter are marked with asterisks). [b] Finally heated 60 min at 80 °C. [c] 5 min at 80 °C + 25 min at 70 °C; d = day(s). [d] Time after the turbidity disappearance. [e] Time after reaching the temperature.

centrations were prepared by diluting the stock solution (1.0×10^{-2} g cm^{-3}) immediately before each measurement.

Rayleigh–Gans–Debye (R–G–D) Light Scattering. For measurement of s-PMMA in BAC, a Fica 50 instrument was used (unpolarized primary beam of wavelength 546.1 nm, angular interval 30–150°). The solutions were purified by filtration through a sintered glass filter G5 (VEB Jenaer Glaswerk, GDR) heated at 80 °C. For evaluation of experimental data, the following temperature dependence of the refractive index increment, dn/dc, in BAC was used:

$$dn/dc = 0.097 + 2.5 \times 10^{-4}(T - 25) \quad (1)$$

where T is the temperature (°C).[16g]

Lorenz–Mie Light Scattering: Ratio Methods.[32-34] Both integral (ITR) and differential (DTR) turbidity ratio methods were used for the characterization of aggregating particles.[35] Turbidities of the s-PMMA–BAC system were measured with a Perkin-Elmer Hitachi UV–vis spectrophotometer (Model 340) at three wavelengths (435.8, 546.1, and 684.3 nm) and two polymer concentrations ($c_0 = 9.0 \times 10^{-3}$ and 4.5×10^{-3} g cm^{-3}) (sample s-PMMA-1). Samples were originally dissolved at 100 °C (24 h) and then kept at 80 °C. The cooling proceeded from 80 or 70 °C to the aggregation temperature, 53, 50, or 48 °C (detailed conditions are given in Table II). The forward-angle dissymmetry method (FAD) was used to recalculate data from measurements performed by the classical R–G–D (angular) light scattering method beyond its validity region. The principles of the individual ratio methods are briefly described below, as they are not currently used.

Integral Turbidity Ratio Method (ITR).[35a-c] This method consists of measuring the turbidities τ_a and τ_b (absolute or relative, i.e., direct photometer readings) at two wavelengths, λ_a and λ_b, which yields for the turbidity ratio

$$T_{ab} = \tau_a(\lambda_a,\alpha_a,m)/\tau_b(\lambda_b,\alpha_b,m) = \kappa^{-2(b-a)}S_a(\alpha_a,m)/S_b(\alpha_b,m) \quad (2)$$

where λ is the wavelength in the medium, $\alpha = \pi L/\lambda$ is the relative size and L is the diameter of the spherical or equivalent scatterers (aggregated particles), m is their relative refractive index, and S is the turbidity function, identical with Heller's Σ.[33] Pairs of λ_a,λ_b and α_a,α_b are bound by the sequence condition of a constant quotient $\kappa = 1.2531$, e.g., λ_0 ($=\lambda_0\kappa^0$) = 326.7 nm, $\lambda_1 = \lambda_0\kappa^1$, $\lambda_2 = \lambda_0\kappa^2$, etc. (corresponding to the wavelength in vacuo: Λ_0 = 435.8, Λ_1 = 546.1, Λ_2 = 684.3 nm, etc.), which allows us to use the same tables for all pairs of wavelengths.[35c] For three turbidity ratios $T_{ab} = T_{01}$, T_{12}, and T_{02} (where, e.g., $T_{01} = \tau_0/\tau_1$), the respective relative sizes α_{01}, α_{12}, and α_{02} may be found from tables;[35c] they are not defined on the same scale (α_{12} is related to the original λ_1 scale; α_{01} and α_{02} are related to the λ_0 scale, the size unit being ~125 and ~100 nm, respectively). Hence, the absolute size (the particle diameter L) may be estimated from the relations $L_{12} \approx \alpha_{12} \times 125$ nm, $L_{01} \approx \alpha_{01} \times 100$ nm, and $L_{02} \approx \alpha_{02} \times 100$ nm; if all dimensions obtained are equal, $L_{01} = L_{12} = L_{02}$, the measured system is monodisperse. Estimation of the concentration of active scatterers (here, aggregated particles), c (g cm^{-3}), and/or of their number N (cm^{-3}) can be performed by inserting the experimental turbidity τ_e (absolute only) into an appropriate relation

$$c = \tau_e/[\tau/c] \tag{3a}$$

$$N = \tau_e/R = 2\pi\tau_e/\lambda^2 S = 4\pi\tau_e/\alpha^2\lambda^2 K \tag{3b}$$

where $[\tau/c]$ is the theoretical specific turbidity (note that the values $[\tau/c]$ in the tables must be multiplied by a factor of 100, as c is expressed in g/100 g),[35c] R is the scattering cross section, $S = 2\pi R/\lambda^2$, and K is the scattering coefficient; the subscript e is used only here to distinguish the experimental turbidity τ_e from the theoretical turbidity. Usually, concentration c (note that $c \leq c_0$) was estimated from the ratio $\tau_e/[\tau/c]$, where experimental τ_e was mostly that for λ_1 and theoretical $[\tau/c]$ was taken from the tables for the relative size α or absolute size $L = \alpha\lambda/\pi$, estimated by the ITR method and adjusted to the λ_1 scale.[35c] For the estimation of N, theoretical data of R, S, or K corresponding to the relative or absolute size found by the ITR method were used; N can be estimated also from the ratio $c/v\rho$ (particle volume, v, is calculated for the respective α, provided that its density ρ is known).

Differential Turbidity Ratio Method (DTR).[35b] Consider a system in which a change occurs (e.g., in the size and number of scatterers) leading to a decrease or increase in turbidity τ with time t. At two arbitrarily chosen times, t_a and t_b, the turbidity τ reaches the values τ_a and τ_b, respectively, which correspond to the states s_a and s_b of the system. At any time, the turbidity contains integral information about the whole system. The principle of additivity is supposed to be valid also for the turbidity response to all events occurring in the system between times t_a and t_b. The situation is simplified if only one process is responsible for the change from s_a to s_b: the difference of turbidities, $\Delta\tau = |\tau_a - \tau_b|$, is coupled with changes in the size and number of those scatterers only which are responsible for the effect observed. Thus, if we measure the turbidity difference between two arbitrarily (but isochronously) chosen states of the system under study at appropriate time intervals and if we treat the differential data (like $\Delta\tau$) instead of the integral data (τ) using the same procedure as in the ITR method, we obtain the respective characteristics of those scatterers which are responsible for such changes within individual time intervals.

Forward-Angle Dissymmetry Method.[35d,36] In contrast with the classical definition of dissymmetry, $z = i_\theta/i_{180-\theta}$, the forward-angle dissymmetry is defined by $\zeta = i_{\theta_1}/i_{\theta_2}$, where $\theta_2 - \theta_1 =$ 10 or 15°, both angles θ lying in the quadrant 0–90°. If we express i_θ in terms of the Lorenz–Mie theory and use the corresponding tables[35d] (or calculations), we can easily obtain the necessary data for constructing the dependences $\zeta = f(\alpha)$ or $\zeta = f(L)$; some of these data are tabulated. In our case, intensities scattered at θ = 30, 45, 60, and 75° were used for calculating the forward-angle dissymmetries $\zeta(30/45)$, $\zeta(45/60)$, and $\zeta(60/75)$; therefrom, the corresponding particle size was found from the respective tables.[35d]

The integral and differential turbidity ratio methods, along with the forward-angle dissymmetry method, have many priorities for aggregation studies, viz., their contactless and continuous measurement. Used in the size range from 100 nm to several micrometers (this depends on the relative refractive index), they are sufficiently reliable, accurate, and fast and are in most respects comparable to the main light scattering methods. Although very simple, they are able to supply data on the size (without the concentration being known), volume, number, and concentration of particles (provided that they are nearly spherical) with a frequency quite sufficient for kinetic measurements. This set of data is dense enough to allow an adequate isochronous interpolation even in the case of fast processes. Limitations of these methods are very similar to those of other light scattering techniques, some of them being partly (multiple scattering) or nearly (concentration dependence) compensated. The turbidity methods are less sensitive than the angular measurements, also against impurities. Data obtained by the ITR and DTR methods are comparable with those of electron microscopy, as their average values lie between the number and weight averages.

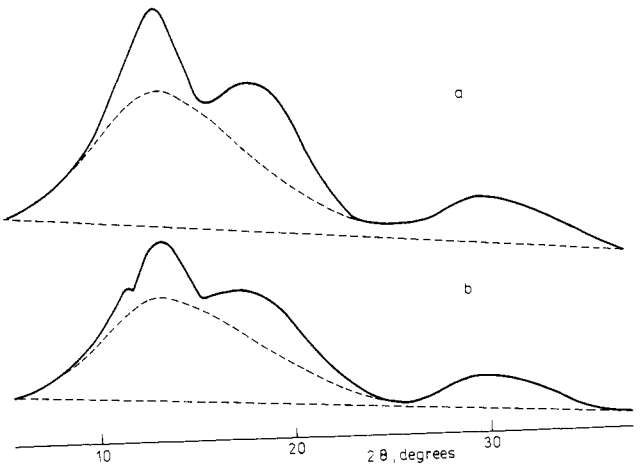

Figure 1. WAXS diagrams for films: (a) s-PMMA-2; (b) s-PMMA-1. Separation of crystalline and amorphous scattering (the latter by dashed curve and line).

III. Results

In order to characterize the aggregation process occurring in the s-PMMA–BAC system in terms of the extent of aggregation (fraction of aggregates) and degree of aggregation (size of aggregates), we used several methods with different capability as to the object and/or the effect observed. This should be taken into account when the results of the individual methods are compared.

Wide-Angle X-ray Scattering (WAXS). The WAXS diagrams of the "dry" samples of s-PMMA-1 and s-PMMA-2, i.e., films prepared by evaporation of BAC from suspensions isolated by centrifugation, have clearly shown that they are partly crystalline (the same samples isolated from acetone solutions were quite amorphous). The separation into crystalline and amorphous scattering is indicated in Figure 1. The crystallinity of samples thus obtained reached 34% for s-PMMA-1 and 29% for s-PMMA-2; this corresponds to the content of syndiotactic triads in the sample (cf. Table I). On the contrary, no crystallinity was found in samples isolated by centrifugation only, i.e., in suspensions with a considerable amount of BAC (>40%).

NMR Spectroscopy. In our preceding papers on aggregation of s-PMMA in solution,[16a–h] the ^{1}H NMR resonances of aggregated units were shown to be so wide that they could not be detected in the high-resolution spectra. The width and shape of bands observed in the high-resolution ^{1}H NMR spectrum are practically unaffected by aggregation; these bands evidently correspond to nonaggregated monomer units. From the point of view of proton mobility, therefore, s-PMMA solution, partly consisting of associated structures, behaves as a two-phase system.[16e] In this system, only s-sequences longer than a certain minimum length[16b,f] participate in association, i.e., undergo

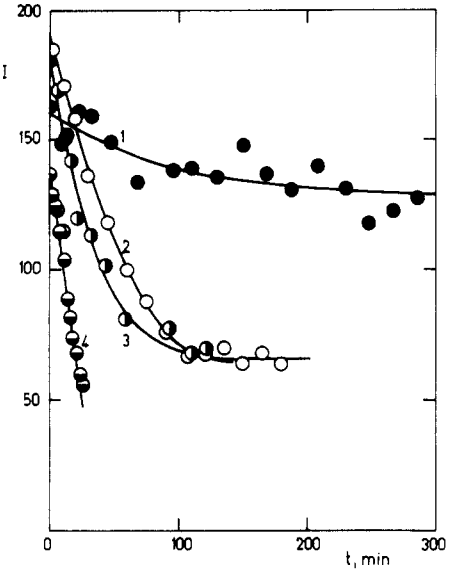

Figure 2. Time dependence of the band intensity of OCH_3 protons, I, of s-PMMA-1 in BAC ($c_0 = 9.0 \times 10^{-3}$ g cm^{-3}). Aggregation temperature T (°C): (1) 51.5; (2) 50.5; (3) 48.5; (4) 46.5.

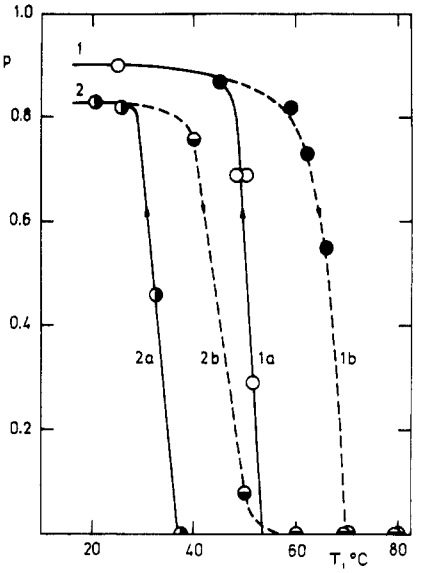

Figure 3. Dependence of the "equilibrium" values of fraction p (aggregated monomer units) on temperature T (°C) of s-PMMA-1 ($c_0 = 9.0 \times 10^{-3}$ g cm^{-3}) in BAC (1a) and toluene-d_8 (2a) and their comparison with a temperature dependence of fraction p during the heating of aggregates formed at 25 °C (curves 1b and 2b).

mutual interaction stable on the NMR time scale. By measuring the time dependence of intensities of high-resolution ^{1}H NMR resonances, it is possible to investigate indirectly the kinetics of aggregate formation.[16f]

In this paper, the aggregation of s-PMMA-1 has been studied in the following temperature intervals: 46.5–51.5 °C (BAC) and 20.5–37.5 °C (toluene-d_8). Only the time dependence of the band intensity of the OCH_3 protons could be studied in BAC, as the bands of CH_2 and α-CH_3 protons were overlapped by strong bands of the solvent. In toluene-d_8, the intensities of all proton bands of s-PMMA were estimated and found to have the same time dependence (see also ref 16c,d,f). As the shift difference between the OCH_3 protons of s-PMMA and the OCH_2 protons of BAC is relatively small (~0.4 ppm), an accurate determination of integrated intensities of OCH_3 is no longer possible and must be replaced by measuring the heights of the OCH_3 band. This is possible, since the widths of these bands are not subjected to changes during aggregation. The fraction p of aggregated monomer units may be estimated from the relation $p = 1 - I/I_0$, where I and I_0 are the respective intensities of the band with and without aggregation occurring in the system.

The time dependence of the peak intensity for OCH_3 protons in s-PMMA-1 in BAC may be seen in Figure 2. All curves were measured under identical conditions and are mutually comparable, because the correction for intensity differences due to temperature is negligible. The lower intensity at time $t = 0$ and temperature 46.5 °C is apparently caused by aggregation already occurring during the period of 3–4 min used for temperature equilibration. The intensity decreases monotonically with time and, when measured for a sufficiently long time, reaches a constant value (e.g., at 50.5 °C, Figure 2). A decrease in intensity without an initial delay period shows clearly that the mobility of the s-PMMA units is limited immediately when the respective aggregation temperature is reached. The aggregation rate increases steeply with the magnitude of the temperature drop (Figure 2). The same behavior has been observed with s-PMMA in toluene-d_8.

Intensities measured after a long time at 51.5 and 50.5 °C are very different (Figure 2), which indicates different p values. After 5 h at 51.5 °C, either $p = 29\%$ (if $I_0 = 180$) or $p = 21\%$ (if $I_0 = 160$) was found, while at 50.5 °C, $p = 64\%$. These values are lower than that obtained at 25 °C ($p = 90\%$, Figure 3). The same trend was observed also with s-PMMA in toluene-d_8. As follows from Figure 3, no perceptible aggregation (i.e., less than a few percent of monomer units) occurs in s-PMMA–BAC ($c_0 = 9.0 \times 10^{-3}$) above 54 °C and in s-PMMA–toluene-d_8 above 37 °C.

A distinct "hysteretic" effect was found when aggregates formed at 25 °C were heated. Figure 3 shows that in both solvents (BAC and toluene-d_8) the given "equilibrium" value of p reached during heating lies at much higher temperature than the aggregation temperature needed for reaching the same "equilibrium" value of p (during the aggregation process).

Viscometry. Experience has shown that the final state of s-PMMA aggregates may be quite different according to the solvent used in the experiment; in toluene, an isorefractive gel is formed, and in BAC, the aggregation leads to flocculation and, eventually, sedimentation. In spite of this, the shape of the time dependence of viscosity was found to be similar in both systems within a time period where the measurement is reliable: viscosity, originally constant, passes through a slight minimum and, after a certain time t_c, begins to rise. The time t_c and the steepness of the increase in viscosity depend on the polymer concentration (Figure 4a) and temperature T (°C) (Figure 4b,c). The most distinct minimum (~10% of specific viscosity) is found for systems with the highest polymer concentration; the minimum disappears in systems with a low polymer concentration and at higher temperatures.

The t_c–T dependence (Figure 5) has a hyperbolic character, the asymptotes being $t_c = 0$ and $T = T_\infty$ (°C), which enables us to extrapolate linearly $1/t_c$ vs. T to zero. This can be utilized for estimation of the temperature T_∞ at which no more aggregation occurs (from the viewpoint of viscometry) in solutions with a given polymer concentration. For $c_0 = 9.0 \times 10^{-3}$ g cm^{-3}, the following T_∞ values have been found: 54 °C (BAC); 41 °C (toluene).

R–G–D Light Scattering and Osmometry. The angular light scattering methods are highly sensitive and effective tools for the characterization of aggregation processes,[37,38] especially at their very beginning, when the solution is completely transparent. Exact evaluation of experimental data via the Zimm plot (and similar tech-

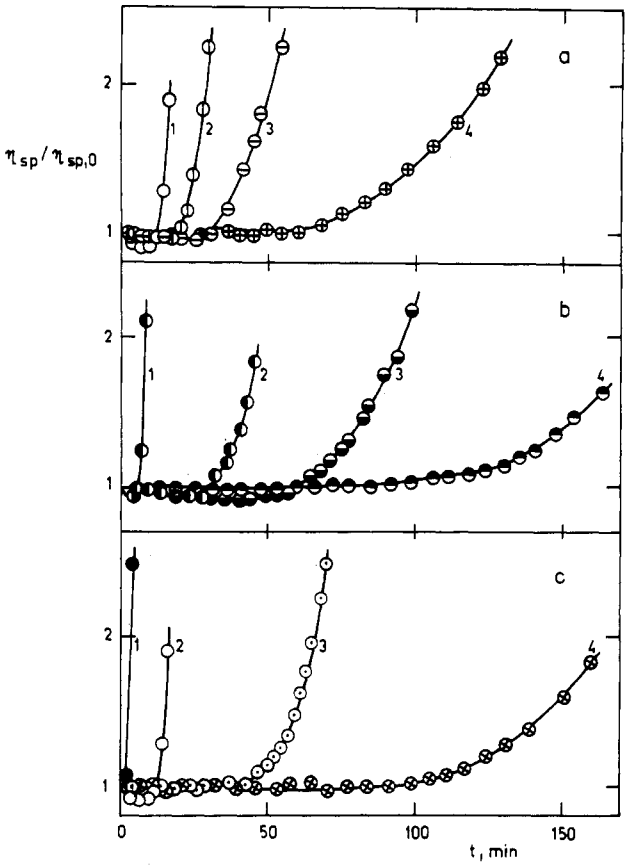

Figure 4. Dependence of $\eta_{sp}/\eta_{sp,0}$ of s-PMM-1 in BAC or toluene on the aggregation time t (min): (a) s-PMMA-1 in BAC (concentration g dL^{-1}): (1) 0.90; (2) 0.45; (3) 0.225; (4) 0.112 (T = 45 °C); (b) s-PMMA-1 in toluene (T (°C): (1) 25; (2) 33; (3) 35; (4) 37.2 (concentration 0.90 g dL^{-1})); (c) s-PMMA-1 in BAC T (°C): (1) 40; (2) 45; (3) 50; (4) 52 (concentration 0.90 g dL^{-1})). T (°C) is the aggregation time; $\eta_{sp,0}$ is related to t = 0 min.

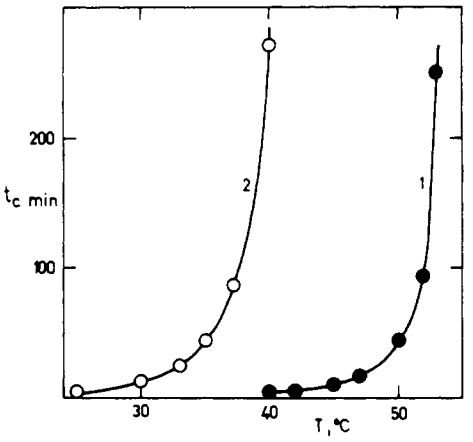

Figure 5. t_c–T diagram for s-PMMA-1 in BAC (1) and toluene (2) (concentration 0.90 g dL^{-1}); t_c is the time corresponding to the steep increase in viscosity.

niques[37]) is impossible, since the course of aggregation depends strongly on the dilution of the system under study. Then only the apparent molecular weight defined by $M_{w,app} = R_0/Kc$ may be calculated from experimental data at a finite concentration c as a suitable characteristic of the degree of aggregation (the dependence on the second virial coefficient, A_2, being neglected). Here, K is the optical constant and R_0 is the Rayleigh ratio extrapolated to zero angle.[38]

Thus, the aggregation of s-PMMA in BAC could be made observable also at elevated temperatures (if there is any) where other methods fail. Therefore, a sample of

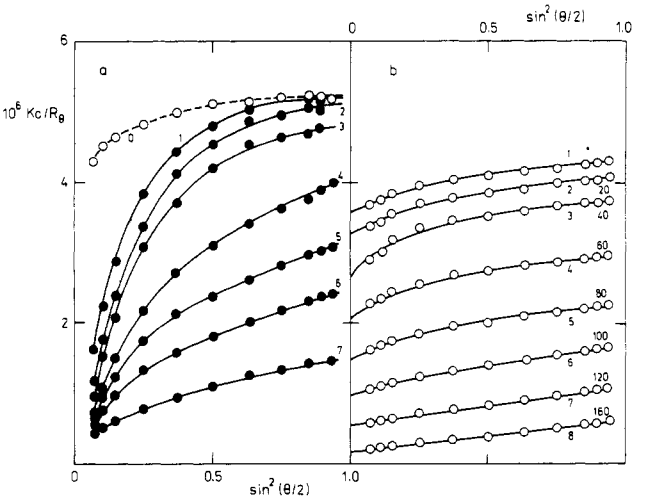

Figure 6. Dependence of the light scattering diagrams on the aggregation time t (min) of s-PMMA in BAC. (a) s-PMMA-2, $c_0 = 1.0 \times 10^{-2}$ g cm^{-3}; heated at 100 °C (curve 0); aggregation temperature T = 60 °C (curves 1–7); aggregation time t (min): (1) 0; (2) 60; (3) 180; (4) 320; (5) 380; (6) 440; (7) 1320. (b) s-PMMA-1, $c_0 = 9.0 \times 10^{-3}$ g cm^{-3}; T = 57 °C; t (min): (1) 0; (2) 20; (3) 40; (4) 60; (5) 80; (6) 100; (7) 120; (8) 160.

s-PMMA-2 ($c_0 = 1.0 \times 10^{-2}$ g cm^{-3}) was heated at 100 °C for 12 h and then measured at this temperature (Figure 6, curve 0). (Its scattering envelope has a smoothly deformed shape at low angles resembling that measured for s-PMMA-2 in chloroform, in which s-PMMA dissolves molecularly;[16g] in both cases, the curvature is probably due to the presence of a few large particles of stable impurities which cannot be excluded under the given conditions. This has no influence on further measurements (curves 1–7), as they can be easily corrected.) The sample was then cooled to 60 °C (time t = 0) and immediately measured (curve 1): while the Kc/R_θ values were nearly identical with curve 0 at higher angles, the scattering envelope at low angles was distinctly curved. As the aggregation continues, the R_θ values increase at higher angles (curves 2–7) and the scattering envelopes are gradually straightened. $M_{w,app}$ estimated by extrapolation from higher angles changes from the initial value 2×10^5 (curves 0 and 1) to 2×10^6 (curve 7), but much larger particles are always present in the system.

The increase in $M_{w,app}$ by one order of magnitude can be seen already after 20 h, while no change in the osmotic pressure Π was noticed after 22 days of aggregation at 60 °C; i.e., the number-average molecular weight, M_n, remained constant from the very beginning to the formation of visible opalescence, signaling the coming macroscopic separation. The dependence $\Pi/RT = c/M_n + A_2c^2$, measured under conditions not too much different from isochronous, keeps its slightly convex character; i.e., the second virial coefficient A_2 for s-PMMA-2 in BAC at 60 °C was always positive (Figure 7). We may conclude that under given conditions only a very small fraction of macromolecules is responsible for the change in $M_{w,app}$.

Investigation of the effect of temperature on the aggregation behavior was performed with the sample s-PMMA-1; this sample was used in all the other methods, and its original scattering envelope was linear. The curvature of the scattering diagram of s-PMMA-1 in BAC at 57 °C is quite slight and disappears with time (Figure 6b). When comparing parts a and b of Figure 6, one should notice very different aggregation rates: at 60 °C the sample after 22 h reached the same aggregation state as that reached at 57 °C already after 120 min (curve 7 in Figure 6b); here, differences in the molecular weight and con-

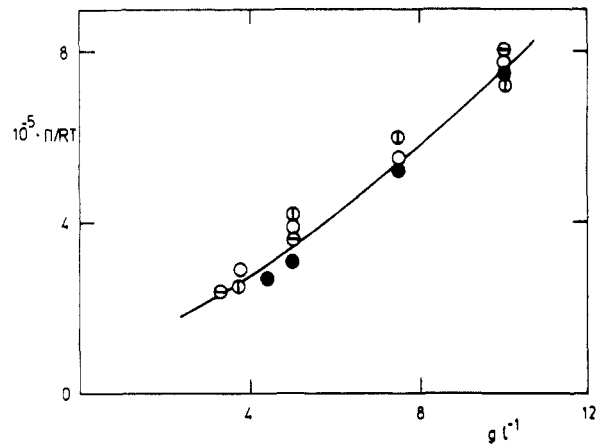

Figure 7. Concentration dependence of the osmotic pressure of s-PMMA-2 in BAC, measured at T = 60 °C; aggregation time t (days): (●) 0; (⊙) 1.25, (⊖) 15; (○) 22.

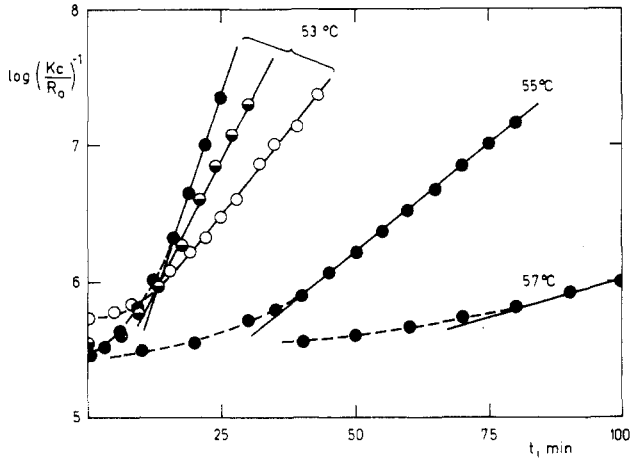

Figure 8. Time dependence of $\log (Kc/R_0)^{-1} \sim \log M_{w,app}$ for various temperatures T (°C) and concentrations c_0 (g cm^{-3}) of s-PMMA-1 in BAC: T = 53, 55, and 57 °C; c_0 (g cm^{-3}): (●) 9.0 × 10^{-3}; (⊖) 4.5 × 10^{-3}; (○) 2.2 × 10^{-3}.

centration of the samples are omitted, since their effect is much lower than that of temperature. The increase in the aggregation rate with decreasing temperature and rising polymer concentration is documented in Figure 8, where the apparent molecular weights, $(Kc/R_0)^{-1}$, are plotted against the aggregation time.

Turbidity. The investigation of the aggregation of s-PMMA-1 in BAC has been performed at two polymer concentrations, 9.0 × 10^{-3} g cm^{-3} (marked by asterisks) and 4.5 × 10^{-3} g cm^{-3}, and with five combinations of thermostating (dissolution) and aggregation temperatures: series A, 70–52 °C; series B, 70–50 °C; series C, 80–50 °C; series D, 70–48 °C; series E 80–48 °C. A typical turbidity dependence on aggregation time is given in Figure 9a. Characteristics defining the aggregation experiments and the respective turbidity curves are collected in Table II. The turbidity curves are S-shaped, provided that the aggregation time is sufficiently long. In the first region, the curve increases relatively slowly and its initial part is not accessible to the ITR and DTR methods (but can be measured by the R–G–D and FAD methods). After passing the more or less distinct bend, the turbidity increases much faster (almost linearly or with a smooth inflection). In the second bend, the increase in turbidity is slowed down, and the system approaches the region of macroscopic precipitation and sedimentation.

The rate of aggregation in the first and mainly in the second region increases distinctly with the polymer con-

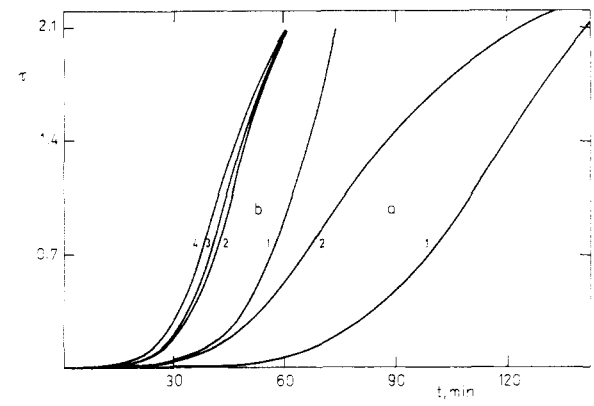

Figure 9. Dependence of turbidity τ on the aggregation time t (min). (a) Sample A1/1-2* (c_0 = 9.0 × 10^{-3} g cm^{-3}), aggregation temperature T = 52 °C. (b) Sample D1/1-4 (c_0 = 4.5 × 10^{-3} g cm^{-3}), T = 48 °C. Experimental conditions are given in Table II.

centration and with the drop in temperature. Data given in Table II confirm this observation: thus, e.g., the aggregation times of sample A1/1* (or C1/1-2) are clearly longer (i.e., the increase in turbidity is slower) than that of B1/2-4* (or E1/2-5); on the contrary, the aggregation times of A1/1* (or B1/2-4*) are distinctly shorter (the turbidity increase is steeper) than that of A2/1 (or B2/1). Just in our first measurements we observed that the aggregation depends strongly on the immediately preceding history of the sample (cf. Table II). Sample A1/1* was kept for a long time at 100 °C, then adjusted to 80 °C (1 h), and before the measurement, adjusted to 70 °C (15 min). The first aggregation cycle (140 min at 52 °C) is illustrated by curve 1, Figure 9a. The sample was heated (the turbidity disappeared within 15 min) and kept for additional 15 min at 70 °C. In the second cycle (128 min at 52 °C), the increase in turbidity appeared much sooner and its course was much steeper. Samples B1/1, B3/1, D1/1, and D3/1 behaved in the same way, so that the effect may be seen as proved. The shapes of the curves in the second and further cycles were close to each other (e.g., D1/1-4, Figure 9b). However, if the sample was kept in the aggregated state at 25 °C for a long time (sample E1/1), the effect was quite opposite—the turbidity reached its highest values in the first cycle. A similar, but less expressive effect was observed with sample C1/1 kept 50 min at 50 °C and then heated to 80 °C.

Turbidity Ratio Methods: Particle Size and Concentration. The measured turbidities contain the whole information about individual scatterers. Since they were estimated at three wavelengths, this condition is satisfactory for determination of the average size of particles and their distribution.[39] However, the aggregation process of s-PMMA in BAC is so complex that the distribution is hardly predictable. Therefore, the average size and concentration of particles were estimated, their system being considered as a set of equivalent spherical scatterers with constant density. A selection from all experimental data (obtained for samples and conditions defined in Table II) is given in Table III, which should document the plausibility of our observations and conclusions. To save space, only some of the data obtained (α, L, c, and N) are given in extenso.

The dependence of the particle size on the aggregation time roughly follows the same dependence of turbidities but becomes S-shaped only if actual precipitation occurs in the system (Figure 10). This dependence indicates that at least two mechanisms are responsible for the effect observed: in the first process, particles under 100 nm in

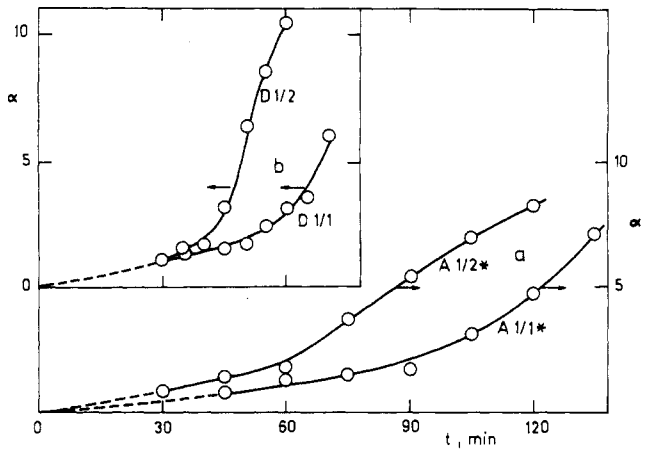

Figure 10. Dependence of the relative particle size α on the aggregation time t (min). (a) Sample A1/1-2* ($c_0 = 9.0 \times 10^{-3}$ g cm^{-3}), aggregation temperature $T = 52$ °C. (b) Sample D1/1-2 ($c_0 = 4.5 \times 10^{-3}$ g cm^{-3}), $T = 48$ °C. Experimental conditions are given in Table II.

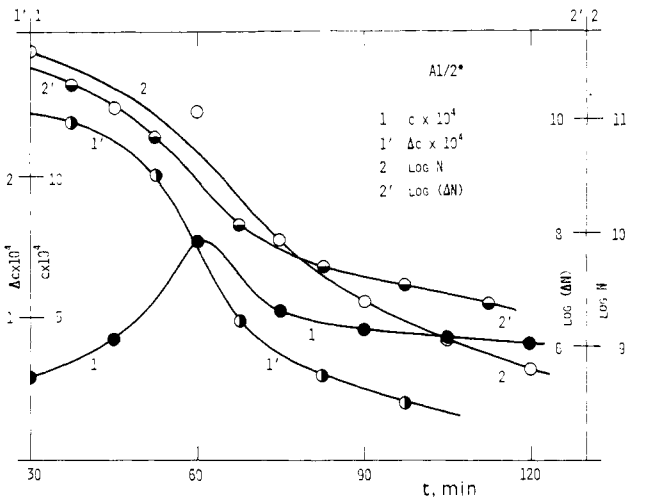

Figure 11. Time dependence of concentration c and number N of aggregated particles: "integral" (c, N) and "differential" (Δc, ΔN) values.

size are active, while the second process gradually leads to particles 1.5 μm in size. From the DTR data, it may be seen that the particles before precipitation and sedimentation are even larger (average size 3 μm—see, e.g., B1/2*). "Critical" size in the first bend region is approximately 200 ± 20 nm.

To confirm data obtained by the ITR and DTR methods and to test the continuity between these and the R–G–D light scattering methods, some data from angular measurements were recalculated in terms of the Lorenz–Mie theory according to the FAD method. In all cases, an isochronous interpolation of experimental data was needed; the results are collected in Table IV. They seem to be quite rational and well matched with those supplied by the turbidity ratio methods.

In almost all cases, particle size rises monotonically with aggregation, as the measurement was usually stopped before appearance of the macroscopic precipitation and sedimentation. The same trend was also indicated by the "differential" data obtained by the DTR method for individual intervals on the aggregation curve. In accordance with expectation, these sizes were considerably greater than indicated by the ITR method (cf. Table III and Figure 11).

A different behavior is shown by the concentration of aggregated particles, c (g cm^{-3}), estimated from the ratio of the experimental turbidity (τ) and the theoretical specific turbidity ($[\tau/c]$) for particles of the relative size α determined by the turbidity ratio method. In all individual or repeated measurements (by the ITR method), the concentration c increases from the beginning of aggregation, sooner or later reaching its maximum, and decreases again to the end. (Note the difference between "concentration of aggregates", c, and "total polymer concentration", c_0.) On the contrary, the "differential" concentrations (i.e., the concentrations of aggregates responsible for a change occurring within the chosen time interval and determined by the DTR method) reach their highest values at the beginning and, with proceeding aggregation, decrease monotonically by about one order of magnitude. The "integral" number of particles (aggregates), N (cm^{-3}), which corresponds to the whole system at a given temperature, is a monotonically decreasing function of the aggregation time (at least in the second region) and its values change by 1–3 orders of magnitude. The same trend has been found for the "differential" values of the number of particles (aggregates), which change by 1–4 orders of magnitude. Their course is much steeper than for the concentration data, because $N \sim c/\alpha^3$, where α rises considerably with time.

IV. Discussion

Model of s-PMMA–BAC Interactions. If a syndiotactic polymer, s-PMMA, is dissolved in a not too good solvent, like n-butyl acetate (BAC), the stability of such a system depends predominantly on its temperature and polymer concentration.[16g] With decreasing temperature, the preference for segment–solvent interactions weakens for one part of the macromolecules in favor of segment–segment contacts, and the system becomes turbid due to polymer separation. With a-PMMA, no such effect can be observed over a large temperature range and BAC still remains a rather good solvent also at lower temperature.[6a,16g] As the content of syndiotactic triads in a-PMMA is relatively large, the different distribution of s-sequences (long s-sequences predominate in s-PMMA while in a-PMMA they are practically absent) seems to be the only structural characteristic which correlates with their dissimilar behavior.[16d] This difference is even decisive for promoting a conformational change after the temperature decrease, probably by ordering appropriate segments into crystallite-like domains: for steric reasons, intramolecular ordering is expected to be preferred, at least in this stage, over intermolecular association by crystalline domains executed by multiple collisions.

The intramolecular ordering by specific interactions of long s-sequences[16e,f] (probably consisting in the formation of more or less developed helices[6b,13]) occurs under conditions when the interaction parameter $\chi < 0.5$, so that the globule or collapsed coil formation in terms of the Lifshitz[40] or Post–Zimm[41] theories, respectively, cannot be made responsible for this effect. Nevertheless, as such coils condensed by intramolecular ordering fulfil requirements postulated for globules,[40] we shall use this designation. We assume that, at a given temperature, only a limited number of chains are able to follow simultaneously the scheme given above. First, only that fraction of macromolecules corresponding to actual "supersaturation" (due to the temperature drop) is allowed to form "crystallites": the "supersaturation" (expressed in terms of s-sequences of specific length and, probably, also of chain length) is the driving force for configurational changes in the polymer molecules leading to nucleation.[23a,b] Furthermore, conformational changes seem to occur immediately after the temperature drop, but their velocity in the individual chains is probably different: being governed by Brownian

Table III
Turbidity τ, Size α, Concentration c, and Number N of Particles in the System of s-PMMA: Some Selected Data[a]

Sample A1/1*

	t												
	45	Δ	60	Δ	75	Δ	90	Δ	105	Δ	120	Δ	135
τ_1	0.034_5	0.119_5	0.154	0.260	0.414	0.454	0.868	0.652	1.520	0.794	2.314	0.691	3.005
α_1	0.80	1.48	1.30	1.69	1.52	3.08	1.72	4.79	3.11	12.2	4.77	15.8	7.11
10^4c	1.50	1.36	2.19	2.38	4.45	1.75	7.79	1.48	5.79	0.74	5.27	0.55	4.49
N	26E10	37E9	19E10	42E9	11E10	52E8	13E10	12E8	17E9	35E6	42E8	12E6	11E8

Sample A1/2*

	t												
	30	Δ	45	Δ	60	Δ	75	Δ	90	Δ	105	Δ	120
τ_1	0.087_5	0.269_5	0.357	0.564	0.921	0.771	1.692	0.650	2.342	0.496	2.839	0.362	3.201
α_1	0.88	1.74	1.44	3.29	1.80	8.54	3.73	12.4	5.43	14.5	6.95	17.3	8.23
10^4c	2.97	2.38	4.22	2.00	7.71	0.97	5.17	0.60	4.63	0.41	4.34	0.27	4.16
N	38E10	39E9	12E10	48E8	11E10	13E7	86E8	27E6	25E8	12E6	11E8	46E5	65E7

Sample A2/1

	t											
	45	Δ	60	Δ	75	Δ	90	Δ	105	Δ	120	
τ_1	0.039	0.039	0.088	0.103	0.191	0.164	0.355	0.237	0.592	0.317	0.909	
α_1		1.72		1.93	1.59	2.93	1.70	5.02	3.08	7.73	3.78	
10^4c				0.78	1.92	0.68	3.22	0.51	2.29	0.44	2.73	

Sample B1/1*

	t												
	30	Δ	35	Δ	40	Δ	45	Δ	50	Δ	55	Δ	60
τ_1	0.168	0.170	0.338	0.272	0.610	0.369	0.979	0.483	1.462	0.587	2.049	0.680	2.729
α_1	0.77	2.97	1.31	2.07	1.45	3.13	1.61	4.60	2.80	6.30	3.16	16.0	4.80
10^4c	3.32	0.69	4.77	1.88	7.12	1.40	9.72	1.15	6.44	0.99	7.66	0.53	6.17
N	56E10	23E8	19E10	18E9	20E10	39E8	20E10	10E8	25E9	34E7	21E9	11E6	48E8

Sample B1/2*

	t														
	25	Δ	30	Δ	35	Δ	40	Δ	45	Δ	50	Δ	55	Δ	60
τ_1	0.173	0.225	0.398	0.355	0.753	0.513	1.266	0.565	1.831	0.506	2.337	0.433	2.770	0.350	3.120
α_1	0.81	1.62	1.25	2.97	1.27	5.37	2.16	10.6	3.39	12.1	4.62	25.2	9.16	P	7.71
10^4c	7.33	2.20	6.12	1.44	11.2	1.03	8.24	0.58	6.26	0.47	5.51	0.31	3.27	P	4.30
N	12E11	45E9	27E9	48E8	21E10	57E7	18E10	42E6	15E9	23E6	48E8	17E5	37E7	P	81E7

Sample B2/1

	t															
	30	Δ	45	Δ	60	Δ	75	Δ	90	Δ	105	Δ	120	Δ	135	
τ_1	0.115	0.362	0.477	0.674	1.151	0.523	1.674	0.359	2.033	0.247	2.280	0.179	2.459	0.131	2.590	0.097
α_1	1.22	3.86	2.88	12.1	6.58	15.4	9.55	15.5	10.7	20.0	12.1	18.8	12.4	20.1	12.7	19.5
10^4c	1.85	1.06	2.02	0.63	1.86	0.42	1.90	0.29	2.08	0.18	2.14	0.13	2.27	0.093	2.33	0.070
N	87E9	16E8	73E8	31E6	56E7	99E5	19E7	67E5	15E7	19E5	10E7	17E5	10E7	10E5	98E6	80E4

Sample C1/1

	t								
	32	Δ	36	Δ	44	Δ	52	Δ	60
τ_1	0.139	0.129	0.262	0.482	0.744	0.856	1.600	1.133	2.733
α_1	0.83	1.52	1.19	1.89	1.48	3.75	2.42	13.8	5.03
10^4c	5.30	1.39	4.48	3.79	8.43	2.59	12.7	0.96	5.87
N	82E10	34E9	23E10	49E9	22E10	42E8	17E10	32E6	40E8

Sample C1/2

	t										
	32	Δ	36	Δ	44	Δ	52	Δ	60	Δ	64
τ_1	0.092	0.117	0.209	0.424	0.633	0.783	1.416	1.119	2.535	0.509	3.044
α_1	0.64	1.88	1.09	1.64	1.42	3.31	2.13	11.7	4.32	22.5	7.38
10^4	7.1?	0.97	4.32	4.09	7.64	2.74	12.7	1.07	6.47	0.36	4.38
N	23E11	14E9	29E10	81E9	23E10	65E8	22E10	58E6	69E8	27E5	94E7

Sample D1/1

	t															
	30	Δ	35	Δ	40	Δ	45	Δ	50	Δ	55	Δ	60	Δ	65	
τ_1	0.039	0.042	0.081	0.066	0.147	0.106	0.253	0.157	0.410	0.219	0.629	0.297	0.926	0.370	1.296	0.426
α_1	1.60		1.31		1.70	1.55	1.55	3.76	1.73	3.37	2.54	5.36	3.16	6.67	3.65	16.4
10^4c	0.39		1.14		1.34	1.11	2.66	0.47	3.63	0.76	3.20	0.60	3.46	0.38	4.06	0.33

Table III (*Continued*)

Sample D1/2

	t												
	30	Δ	35	Δ	40	Δ	45	Δ	50	Δ	55	Δ	60
τ_1	0.196	0.179	0.375	0.270	0.645	0.357	1.002	0.433	1.435	0.350	1.785	0.271	2.056
α_1	1.13		1.60	4.45	1.78	7.80	3.24	17.5	6.49	16.3	8.58	19.6	10.5
10^4c	3.72		3.73	0.67	5.48	0.49	3.63	0.32	2.35	0.27	2.23	0.19	2.14

Sample D3/1

	t								
	18	Δ	22	Δ	26	Δ	30	Δ	34
τ_1	0.097	0.223	0.320	0.463	0.783	0.801	1.584	1.103	2.687
α_1	1.22	1.86	1.35	2.45	1.59	3.98	2.94	11.1	4.63
10^4c	1.57	1.79	4.27	2.49	7.90	2.26	7.21	1.10	6.33

Sample D3/2

	t								
	12	Δ	16	Δ	20	Δ	24	Δ	28
τ_1	0.387	0.797	1.184	0.888	2.072	0.604	2.676	0.432	3.108
α_1	1.45	3.90	2.98	9.40	4.42	14.0	6.30	15.8	7.35
10^4c	4.55	2.30	4.79	1.02	5.15	0.51	4.52	0.34	4.50

Sample E1/1

	t						
	18	Δ	22	Δ	26	Δ	30
τ_1	0.244	0.516	0.760	0.861	1.621	1.142	2.763
α_1	1.34	3.02	1.74	3.72	2.65	12.6	5.25
10^4c	3.29	2.04	6.69	2.63	7.74	1.03	5.66

Sample E1/2

	t								
	22	Δ	26	Δ	30	Δ	34	Δ	36
τ_1	0.256	0.412	0.668	0.723	1.391	1.054	2.445	0.515	2.960
α_1	1.17	2.49	1.49	4.15	2.15	10.5	4.04	14.2	5.57
10^4c	4.51	3.09	7.46	1.94	9.11	1.09	6.76	0.40	5.69

[a] Only data related to Λ_1 = 546.1 nm are given. Under Δ are data estimated by the DTR method, i.e., $\Delta\tau$ and other differential quantities calculated by means of them. Polymer concentration c_0: 4.5×10^{-3} and 9.0×10^{-3} g cm^{-3} (the latter marked by an asterisk as in A1/1*). For definition of samples, series A–E, see Table II. *t* is the aggregation time (min); 26E10 = 26×10^{10} etc.; P means macroscopic precipitation.

motion (allowing or limiting their existence), the chain rearrangement adequate for "crystallite" formation may be completed within a time ranging from very short (if preorganization exists) to considerably long in the case of lower order. Intramolecular ordering leads to a considerable stiffening of some chain segments with a cooperative protective effect against thermal disturbance; this is necessarily accompanied by a distinct change in the free energy of chain and by reduction of the particle size (condensation). Such globules are supposed to be primary particles randomly distributed in the system and initiating aggregation. Also, formation of globules consisting of two chains may be expected if the collision (interpenetration) and "globulation" coincide.

Intermolecular association and aggregation follow immediately after individual globules have been formed, so that both the globule-forming and aggregating particles are present in the system for some time: there seem to coexist individual chains with shorter s-sequences (which are not allowed to form stable contacts in globules), nucleating globules (forming partly reversible aggregates), and aggregating particles, which tend to flocculate. Aggregation is supposed to be achieved by globule–globule, globule–aggregate, and aggregate–aggregate interactions. Also considered is the "crystalline" attachment of an appropriate chain to the colliding globule or aggregate, followed by rearrangement of the chain conformation and by formation of new segment–segment contacts. All these processes should raise the polydispersity of the system. For thermodynamic reasons, each particle tends to minimize its surface, so that small particles are growing preferentially. Such a mechanism would be more probable in the early stages of globule aggregation; however, "fractionation" (i.e., the preference of longer s-sequences or chains in globule formation and aggregation) may disturb this picture.

Regarding the complexity of the system studied, it can hardly be expected that its behavior will be simple and ideal. Flocculation may be seen as a process governed by the Smoluchowski theory,[23] but deviations are also very probable due to the competing interactions. Further fate of flocculates is—sooner or later, but necessarily—connected with sedimentation, i.e., directly or through deswelling of gellike structures.[23]

This qualitative model of s-PMMA–BAC interactions, being compared with recent progress and our experimental results, is discussed in the following sections.

Primary Process ("Globulation"). The most striking picture related to the very beginning of the s-PMMA–BAC interaction is probably that arising from a comparison of NMR and turbidity data (Figure 12). While curve 1 records a steep increase in the fraction *p* of immobilized monomer units with time, the turbidity data refer to a relatively slow aggregation of particles (cf. also Figure 9 and Table III) in the initial region of the aggregation curve. This confrontation shows that the process responsible for a steep increase in *p* immediately after the temperature drop is predominantly intramolecular in nature (formation

Table IV
Particle Size Estimated by the FAD Method Using the Isochronous Interpolation

aggregation		size L (nm) estimated from the FA dissymmetry		
T, °C	t, min	$\zeta(30/45)$	$\zeta(45/60)$	$\zeta(60/75)$
47	7	194	164	154
47	10	166	196	166
53	29	116[a]	136[a]	135[a]
53	35	188[a]	192[a]	180[a]
53	35	208	206	187

[a] Data estimated directly (without isochronous interpolation). $\zeta(30/45)$ is the FA dissymmetry estimated from the ratio of intensities scattered at 30 and 45°, T is the aggregation temperature, and t is the aggregation time.

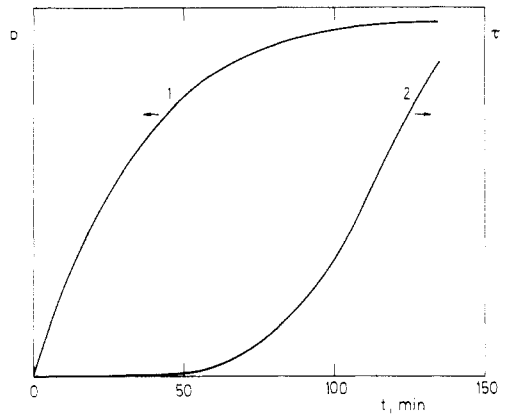

Figure 12. Correlation of (1) p–t and (2) τ–t curves; p is the fraction of immobilized monomer units, τ is the turbidity, and t is the aggregation time (min), p and τ being expressed in arbitrary units. (1) T = 48.5 °C, (2) T = 48 °C; $c = 9.0 \times 10^{-3}$ g cm^{-3}. Cf. Figures 2 and 9.

of double-chain globules is not excluded). Hence, in the limit for time $t \rightarrow 0$, the process is obviously connected with individual particles only.

The velocity of this process leads to the conclusion that the following mechanisms could be made responsible for the immobilization of monomer units in the extent observed: (a) intramolecular ordering (helix, double-helix, or "crystallite" formation) and segment–segment binding; (b) participation of many chains in the process. The former process is very probable, being theoretically substantiated[42] and experimentally evidenced, at least in the solid state.[13c] In solutions and dispersions, the internal order seems to be loosened to some extent, depending on the content of the solvent: by WAXS, the crystallinity was found in films (with ~5% BAC), but not in a suspension (containing more than 40% BAC). The latter process is limited by "supersaturation" of the system after the temperature drop. Preferably, long s-sequences with favorable mutual ordering are to be treated by conformational rearrangement. The increase in the "equilibrium" values of p with decreasing temperature, as found by NMR spectroscopy, indicates that further (shorter) s-sequences interact. These contacts are stable if the interaction energy prevails over the thermal energy of molecular motion, and this is fulfilled only for s-sequences longer than a certain minimum length corresponding to the given temperature and solvent (in toluene at 25 °C, 7–8 monomer units[16f]). The existence of limits ("equilibria") of the NMR p values rising with decreasing temperature may be seen as evidence for that the aggregation process is governed by "supersaturation" (expressed in terms of longer or shorter s-sequences). This does not mean that the number of contacts is directly or simply proportional to the concentration of aggregates. However, the L–M scattering data (Table III) indicate that, with decreasing temperature, the rate of aggregation increases from the very beginning: more globules are engaged in the process. Unfortunately, no adequate data on final conversion to aggregates can be obtained by this method.

The concept of globule formation and aggregation seems to be supported also by viscosity data: soon after the start of the s-PMMA–BAC interaction, by temperature drop, a small but distinct viscosity minimum (~10%) has been observed, followed by a constant viscosity region till t_c (Figure 4). The decrease in specific viscosity η_{sp} may be explained either by a purely intramolecular aggregation process (leading to a more compact conformation) or by an intermolecular aggregation process if the aggregates are more compact than the nonaggregated molecules.[43] For solution without aggregation, we write

$$(\eta_{sp})_1 = [\eta]_1 c(1 + k_H[\eta]_1 c) \quad (4)$$

where $[\eta]_1$ is the intrinsic viscosity of nonaggregated molecules (unimers) and k_H is the Huggins coefficient. For solution containing unimers and dimers, k_H in eq 4 is to be replaced by $k_{H,2}$ which is

$$k_{H,2} = k_H + (2K_1/[\eta]_1 M_1)([\eta]_2/[\eta]_1 - 1) \quad (5)$$

where M is the molecular weight and K is the association equilibrium constant; subscripts 1 and 2 are related to the unimers and aggregates respectively.[44]

If only the intramolecular aggregation took place, the value of $[\eta]_1$ would be decreased and would lead to a decrease in η_{sp}. This process may be compared with intramolecular cyclization. Kuhn and Majer have shown[45] that, if ring formation is a random process, one intramolecular ring amounting, on the average, to about 30 statistical segments reduces the intrinsic viscosity by about 5%. A decrease of 10% would require formation of two rings. If, on the other hand, all the rings are small, the effect on the intrinsic viscosity is much less pronounced, so that a decrease of 10% would be brought about by a large number of intramolecular rings.

Let us consider the second possibility, i.e., intermolecular aggregation (in the dimer approximation). It follows from eq 5 that the specific viscosity of an aggregating system, η_{sp}, can be lower than that of a nonaggregated system, $\eta_{sp,0}$, only if $k_{H,2} < k_H$. It follows from eq 4 that in this case $[\eta]_2 < [\eta]_1$, which means that the effective hydrodynamic volume of dimers is lower than that of unimers. This is possible only if the dimers are compact, i.e., if the number of more or less permanent contacts between aggregated chains is rather high.

Both processes can lead to a decrease in η_{sp}. The idea that multiple permanent contacts are formed either intramolecularly or intermolecularly is compatible with the findings of NMR and light scattering methods (Figure 12).

Secondary Process (Nucleation). There are several reasons for the statement that association of individual particles (condensed chains, i.e., globules) starts immediately after their conformational rearrangement has been completed. Once formed, the globules are particles with a considerably lower free energy (due to their internal ordering and increased preference of the segment–segment interactions leading to partial desolvation and decrease in size), which are also able to interact mutually by multiple Brownian collisions. "Supersaturation", diffusion, and collision efficiency are the main factors governing the process in its extent and velocity. Distribution in the "birth" of globules and partial reversibility of their asso-

ciations lead to retardation of the process. Particles that reached their "critical" size do not dissociate and are in an unstable equilibrium with their parent phase; they are denoted as nuclei. Afterward, aggregation ensues with irreversible growth of the particles (at a given temperature). (Cf. ref 23 and 24.)

Only one of our methods is able to distinguish between formation of globules and their association (aggregation), i.e., the angular R–G–D light scattering method, which is much more sensitive to the intermolecular process than to the intramolecular rearrangement. Thus, it should be possible to obtain quantitative results by combining both light scattering and NMR data. Unfortunately, the existing equipment is not adjusted for adequate measurement, which requires, in particular, a substantial reduction of the thermostating time (now 2–4 min) and for a much faster recording of the light scattering data.

In order to show that the expected nucleation does indeed occur in the system, a very slow aggregation regime (60 °C, $c_0 = 1.0 \times 10^{-2}$ g cm^{-3}) has been chosen (Figure 6a). The presence of large particles is indicated by a strong downward curvature of the scattering envelope obtained immediately after the temperature drop from 100 to 60 °C. Curve 1 shows also clearly that the majority of chains remain with their original molecular weight corresponding to Kc/R_θ values at higher angles (where curves 0 and 1 are nearly identical). With proceeding nucleation, the apparent average molecular weight obtained from higher angles becomes larger (by a factor of 10 for curve 7), still remaining in the size domain expected for nucleation. To demonstrate that the size increase is related only to a small fraction of the polymer dissolved in BAC, the number-average molecular weight of the system was measured osmometrically for a long time: no change in molecular weight was indicated, showing that the fraction of aggregates is much lower than the 1% detectable by this method under the given conditions, in agreement with the NMR results (Figure 3).

In the system where aggregation is much faster (57 °C, $c_0 = 9.0 \times 10^{-3}$ g cm^{-3}), no such effect appears, being overlapped by a large contribution from increasing aggregates (Figure 6b). The curvature at low angles shows that larger aggregates are also present in the system than corresponds to Kc/R_θ values at higher angles.

Indirect evidence for the existence of fairly stable particles has been obtained from measurements by the L–M light scattering methods. If the turbidity of an aggregating system is measured with a sample heated at 80 or 70 °C either to the disappearance of turbidity or for a much longer time, two different pictures may be obtained after the temperature drop (Figure 9): in the former case, the main increase in turbidity starts much sooner than in the latter, where the increase is less steep and higher turbidity may be achieved without macroscopic precipitation. The responsibility for this effect has been ascribed to the existence of nuclei or their predecessors which survived the solvation at higher temperature for a limited time (usually, turbidity disappeared within 15 min). Their higher resistance may be explained by a conformational rearrangement of chains (at least of those inside the aggregate), leading to their lower free energy and inducing a cooperative protective effect against disturbance.

If identified with the mean particle size corresponding to the bend on the α–t curve (Figure 10), the "critical" size of nuclei may be localized, for all cases measured, to 200 ± 20 nm. The monotonic increase in size in the first region leads to values lying between 100 and 200 nm (first deviation from monotonic behavior).

Tertiary Process (Flocculation). After passing the first region on the S-shaped curve (Figure 9), turbidity starts to increase much more steeply; also, the "integral" average particle size roughly follows the same dependence, being shifted to higher times. This can be easily explained by inspection of the "differential" data for α_1 in Table III: they are much higher than the "integral" data, indicating that only a small fraction of (much) larger particles (cf. "differential" concentration and size) is responsible for the major part of the increase in the "integral" average particle size in the whole system. This observation was confirmed without any exception in all measurements performed.

Thus, we may complete our concept of s-PMMA aggregation by a further step: Particles forming during the nucleation period (first region) gradually reach their "critical" size by passing through the first bend. As their interactions are no longer reversible, the rate of aggregation increases considerably (by a factor of 10, in the case of curve A1/1*), being governed (retarded) by the gradual formation of new nuclei capable of irreversible aggregation. However, this may be moderated by "equisizing" of particles, the effect already mentioned and known also as Ostwald's ripening.[23b] If such nuclei or their predecessors (aggregates in an advanced state of nucleation) are already present in the system, e.g., being originated by aggregation at lower temperature and surviving its increase, the flocculation may start much earlier (Figure 9), the flocculates are larger, and their sedimentation appears sooner (cf. Table III).

In order to characterize the rapid flocculation of particles in the s-PMMA–BAC system, the Smoluchowski theory[23] was used for such system. The rate of flocculation expressed by the decrease in the total number of particles, N, per second is given by

$$-\mathrm{d}N/\mathrm{d}t = k'N^2 \tag{6}$$

where k' is the rate constant and t is time; after integration ($N = N^0$ at $t = 0$)

$$1/n = 1/N^0 + k't \tag{7}$$

The slope of the $1/N$ vs. t plot for rapid flocculation is to be compared with that predicted by the Smoluchowski theory. The theoretical value of k', i.e. k_0', may be calculated from the relation $k_0' = 8\pi Da$ by inserting the Einstein expression $D = kT_0/6\pi\eta a$ (where D is the Boltzmann constant, T_0 is the absolute temperature, and η is the viscosity of the medium).

For our samples and conditions, the following rate constants $k' \times 10^{12}$ (cm^3 s^{-1}) were obtained: 0.75 (A1/1*); 0.70 (A1/2*); 0.53 (B1/1*); 4.1 (B1/2*); 0.51 (C1/1); 3.8 (C1/2). The Smoluchowski constant $k_0' = 11 \times 10^{-12}$ cm^3 s^{-1}. This theory takes into account attraction on contact only. The results obtained are considerably lower than those predicted by the theory; data obtained for aggregates nearer to precipitation (B1/2* and C1/2) are in acceptable agreement with k_0'. The rate is far from being constant; k' decreases considerably when returning to the beginning of flocculation. The tendency to reversibility and to week gellike binding by individual chains might be made responsible for such behavior of aggregates.

The flocculation of particles in the s-PMMA–BAC system may be considered to be a very complicated process. The number of particles estimated by our methods and the kinetics of their decrease seem to be quite reasonable (Table III). Other characteristics, such as "differential" data on both number and concentration, also have the expected progress (Figure 11). The more striking is the appearance of a distinct decrease in the "integral"

concentration (Table III and Figure 11) showing a maximum on the c–t curve. A full explanation is not easily found, as the cause of this effect may be in the method, the model, or the system itself.

Method. The specific turbidity ($[\tau/c]$), being the basic quantity, reaches its maximum at $\alpha = 22.5$ (for our conditions), decreases further, and in the interval $\alpha = 55$–90 remains nearly constant. This means that the particles with a size $\alpha > 22.5$ have a lower scattering power; as a consequence, the estimated concentrations are somewhat lower than those (real) observed if the effect were absent. This can be taken into account for the gross flocculates only, but here another effect occurs, viz., sedimentation.

Model. Flocculates are considered as spherical particles of constant density. With an increase in size, the flocculates become probably less dense, individual aggregates (nuclei) and chains being bound in a network. If the particle density is lower, the turbidity ratio method indicates an increase in the particle size, provided that they are larger than a certain size, i.e., $\alpha_{01} > 3.10$, $\alpha_{12} > 3.10$, and $\alpha_{02} > 3.65$. The difference is usually very small, but it increases with the particle size; instead of $\alpha = 20$, $\alpha = 26$ will be found. With the largest particles, this effect could contribute to, but not prevail in, the explanation of the anomaly observed in the c–t curve.

System. In their advanced stage, the flocculates were shown to be very polydisperse. This seems to be a consequence of "fractionation" during the globule formation and nucleation. Also, flocculates seem to grow gradually (probably with some structural rearrangements) until they reach the "critical" size for sedimentation, i.e., when the Brownian motion is no more able to resist gravitation. (Here, it is necessary to stress that this study deals with an unstirred system, which behaves quite differently from the stirred one.) The largest estimated particles have the average size $\alpha = 20$–25, so that the "critical" size for sedimentation might be $\alpha = 28$–30, i.e., 3.5–4.0 μm (respecting corrections mentioned above).

In our opinion, sedimentation is the factor responsible for a major part of the decrease in concentration in the c–t curve. This statement is corroborated by data in Table III: Whenever a major reduction in the "integral" concentration occurs, a very pronounced increase in particle size in the respective time interval may be observed (see the "differential" data for α_1); this indicates that the particles responsible for this change have also a broad size distribution which leads to sedimentation of the largest particles in the same time interval where the "apparent" decrease in the "integral" concentration occurs.

Some structural rearrangements seem to occur also in the precipitate (sediment); this can be documented by an NMR experiment (Figure 3). The "equilibrium" values of p were measured gradually at several temperatures (the lowest being 25 °C) in the cooling and heating periods. It was found that the same "equilibrium" value of p would be reached in the heating period at higher temperature (on the average, by 16 °C for BAC and 12 °C for toluene) than in the cooling period. Obviously, the precipitate with such history became more stable against thermal disturbance (partial disaggregation or dissolution) due to structural rearrangements continuously raising its stability. This is in agreement with the WAXS data obtained for films prepared from precipitates (~5% BAC). Thus, through countless local instabilities within nucleation and flocculation, the system tends to higher stability also during aging of the precipitate.

Acknowledgment. We are indebted to Dr. M. Bohdanecký for stimulating discussions and to Dr. J. Trekoval for kind supply of samples.

Registry No. s-PMMA, 25188-97-0.

References and Notes

(1) Outer, P.; Carr, C. I.; Zimm, B. H. *J. Chen.. Phys.* **1950**, *18*, 830.
(2) Danusso, F.; Moraglio, G. *J. Polym. Sci.* **1957**, *24*, 161.
(3) Liu, H. Z.; Liu, K. I. *Macromolecules* **1968**, *1*, 157.
(4) Tsvetkov, V. N.; Skaska, V. S.; Krivoruchko, N. M. *Vysokomol. Soedin.* **1960**, *2*, 1045.
(5) Watanabe, W. H.; Ryan, C. F.; Fleisher, P. G.; Garret, B. S. *J. Phys. Chem.* **1961**, *65*, 896.
(6) (a) Kirste, R.; Schulz, G. V. *Z. Phys. Chem. (Wiesbaden)* **1961**, *27*, 301. (b) Kirste, R.; Wunderlich, W. *Makromol. Chem.* **1964**, *73*, 240. (c) Schulz, G. V.; Wunderlich, W.; Kirste, R. *Ibid.* **1969**, *123*, 51.
(7) (a) Fox, T. G.; Cohn-Ginsberg, E.; Mason, H. F. *Polymer* **1962**, *3*, 97. (b) Krause, S.; Cohn-Ginsberg, E. *Ibid.* **1962**, *3*, 565. (c) Krause, S.; Cohn-Ginsberg, E. *J. Chem. Phys.* **1963**, *67*, 1922.
(8) Sakurada, I.; Nakajima, A.; Youshizaki, D.; Nakamae, K. *Kolloid Z. Z. Polym.* **1962**, *186*, 41.
(9) (a) Cowie, J. M. G.; Wiles, D. M.; Bywater, S. Paper presented at the Canadian High Polymer Forum, Ste. Marguerite, 1964. (b) Bywater, S. *J. Polym. Sci., Part C* **1970**, *30*, 135.
(10) (a) Liquori, A. M.; Anzuino, G.; Coiro, V. M.; D'Alagni, M.; de Santis, P.; Savino, M. *Nature (London)* **1965**, *206*, 358. (b) Liquori, A. M.; de Santis, P.; Savino, M.; D'Alagni, M. *Polym. Lett.* **1966**, *4*, 943.
(11) Chiang, R.; Burke, J. J.; Threlkeld, J. O.; Orofino, T. A. J. *J. Phys. Chem.* **1966**, *70*, 3591.
(12) van den Berg, W. B.; Hymans, B.; Piet, P.; Heikens, D. *Nature (London)* **1968**, *217*, 949.
(13) (a) Tadokoro, H.; Chatani, Y.; Kusanagi, H.; Yokoyama, M. *Macromolecules* **1970**, *3*, 441. (b) Kusanagi, H.; Tadokoro, H.; Chatani, Y. *Ibid.* **1976**, *9*, 531. (c) Kusuyama, H.; Takase, M.; Higashihata, Y.; To Seng, H.; Chatani, Y.; Tadokoro, H. *Polymer* **1982**, *23*, 1256.
(14) Borchard, W.; Pyrlik, N.; Rehage, G. *Makromol. Chem.* **1971**, *145*, 169. (b) Borchard, W.; Kalawrytinos, G.; Mohadjer, B.; Pyrlik, M.; Rehage, G. *Angew. Makromol. Chem.* **1973**, *29/30*, 471. (c) Pyrlik, M.; Borchard, W.; Rehage, G.; Uerpmann, E. P. *Ibid.* **1974**, *36*, 133.
(15) (a) Buter, R.; Tan, Y. Y.; Challa, G. *J. Polym. Sci., Polym. Chem. Ed.* **1973**, *11*, 2975. (b) Gons, J.; Vorenkamp, E. J.; Challa, G. *Ibid.* **1975**, *13*, 1699. (c) Feitsma, E. L.; de Boer, A.; Challa, G. *Polymer* **1975**, *16*, 515. (d) Challa, G.; de Boer, A.; Tan, Y. Y. *Int. J. Polym. Mater.* **1976**, *4*, 239. (e) de Boer, A.; Challa, G. *Polymer* **1976**, *17*, 633. (f) Vorenkamp, E. J.; Bosscher, F.; Challa, G. *Ibid.* **1979**, *20*, 59. (g) Bosscher, F.; Keekstra, D. W.; Challa, G. *Ibid.* **1981**, *22*, 124. (h) Vorenkamp, E. J.; Challa, G. *Ibid.* **1981**, *22*, 1705.
(16) (a) Spěváček, J.; Schneider, B. *J. Polym. Sci., Polym. Lett. Ed.* **1974**, *12*, 349. (b) Spěváček, J.; Schneider, B. *Makromol. Chem.* **1974**, *175*, 2939. (c) Spěváček, J.; Schneider, B. *Ibid.* **1975**, *176*, 3409. (d) Spěváček, J. *J. Polym. Sci., Polym. Phys. Ed.* **1978**, *16*, 523. (e) Spěváček, J.; Schneider, B. *Polym. Bull.* **1980**, *2*, 227. (f) Spěváček, J.; Schneider, B.; Bohdanecký, M.; Sikora, A. *J. Polym. Sci., Polym. Phys. Ed.* **1982**, *20*, 1623. (g) Mrkvičková, L.; Stejskal, J.; Spěváček, J.; Horská, J.; Quadrat, O. *Polymer* **1983**, *24*, 700. (h) Spěváček, J.; Schneider, B.; Baldrian, J.; Dybal, J.; Štokr, J. *Polym. Bull.* **1983**, *9*, 495. (i) Spěváček, J.; Schneider, B.; Dybal, J.; Štokr, J.; Baldrian, J.; Pelzbauer, Z. *J. Polym. Sci., Polym. Phys. Ed.*, in press.
(17) Katime, I.; Ramiro, V. C.; Figueruelo, J. E. *Eur. Polym. J.* **1977**, *15*, 451.
(18) Jenkins, R.; Porter, R. S. *Adv. Polym. Sci.* **1980**, *36*, 1.
(19) Tsuchida, E.; Abe, K. *Adv. Polym. Sci.* **1982**, *45*, 1.
(20) *Discuss. Faraday Soc.* **1966**, *42*.
(21) *Faraday Discuss. Chem. Soc.* **1978**, *65*.
(22) Fitch, R. M., Ed. "Polymer Colloids II"; Plenum Press: New York and London, 1980: (a) Heller, W., p 153; (b) Croucher, M. D.; Hair, M. L., p 497; (c) Goodall, A. R.; Wilkinson, M. C.; Hearn, J., p 629.
(23) Parfitt, G. D., Ed. "Dispersion of Powders in Liquids"; Applied Science Publishers: London, 1981: (a) Parfitt, G. D., p 1; (b) Füredi-Milhofer, H.; Walton, A. G., p 203.
(24) Ottewill, R. H. *J. Colloid Interface Sci.* **1977**, *58*, 357.
(25) Russel, W. B. *J. Rheol.* **1980**, *24*, 287.
(26) Lips, A.; Willis, E. *J. Chem. Soc., Faraday Trans. 1* **1973**, *69*, 1226.
(27) (a) Lichtenbelt, J. W. Th.; Ras, H. J. M. C.; Wiersema, P. H. *J. Colloid Interface Sci.* **1974**, *46*, 522. (b) Lichtenbelt, J. W. Th.; Pathmamanoharan, C.; Wiersema, P. H. *Ibid.* **1974**, *49*, 281.

(28) Zeichner, G. R.; Schowalter, W. R. *J. Colloid Interface Sci.* **1979**, *71*, 237.
(29) Sato, T.; Sieglaff, C. L. *J. Appl. Polym. Sci.* **1980**, *25*, 1781.
(30) Nieuwenhuis, E. A.; Pathmamanoharan, C.; Vrij, A. *J. Colloid Interface Sci.* **1981**, *81*, 196.
(31) Vogelsberger, W. *J. Colloid Interface Sci.* **1982**, *88*, 17.
(32) van de Hulst, H. G. "Light Scattering by Small Particles"; Wiley: New York, 1957.
(33) Wallach, M. L.; Heller, W. *J. Chem. Phys.* **1961**, *34*, 1796.
(34) Kerker, M. "The Scattering of Light and Other Electromagnetic Radiation"; Academic Press: New York, 1969.
(35) (a) Sedláček, B.; Koňák, Č. *J. Colloid Interface Sci.* **1982**, *90*, 60 and literature cited therein. (b) Sedláček, B.; Zimmermann, K. *Polym. Bull.* **1982**, *7*, 531. (c) Sedláček, B.; Verner, B.; Bárta, M.; Zimmermann, K. *Collect. Czech. Chem. Commun.* **1979**, *44*, 2064. (d) Sedláček, B. *Ibid.* **1971**, *36*, 2625.
(36) Maron, S. H.; Pierce, P. E. *J. Polym. Sci., Part C* **1969**, *27*, 183.
(37) Huglin, M. B., Ed. "Light Scattering from Polymer Solutions"; Academic Press: London and New York, 1972.
(38) Elias, H.-G. "Macromolecules, Structure and Properties"; Wiley: New York, 1977; Vol. 1.
(39) Zollars, R. L. *J. Colloid Interface Sci.* **1980**, *74*, 163.
(40) Lifshitz, I. M.; Grosberg, A. Yu.; Khokhlov, A. R. *Rev. Mod. Phys.* **1978**, *50*, 683. (a) Lifshitz, I. M. *Zh. Eksp. Teor. Fiz.* **1968**, *55*, 2408.
(41) (a) Post, C. B.; Zimm, B. H. *Biopolymers* **1982**, *21*, 2123. (b) Post, C. B.; Zimm, B. H. *Ibid.* **1982**, *21*, 2139.
(42) (a) Flory, P. J.; Sundararajan, P. R.; DeBolt, L. C. *J. Am. Chem. Soc.* **1974**, *96*, 5015. (b) Sundararajan, P. R.; Flory, P. J. *Ibid.* **1974**, *96*, 5025.
(43) Belnikevitch, N. G.; Mrkvičková, L.; Quadrat, O. *Polymer* **1983**, *24*, 713.
(44) Wolff, C.; Silberberg, A.; Priel, Z.; Layec-Raphalen, M. N. *Polymer* **1979**, *20*, 281.
(45) Kuhn, W.; Majer, H. *Makromol. Chem.* **1956**, *18/19*, 239.

Structure of Poly(diacetylenes) in Solution†

Gerhard Wenz, Michael A. Müller, Manfred Schmidt, and Gerhard Wegner*

Institut für Makromolekulare Chemie, Universität Freiburg, D-7800 Freiburg i.Br., West Germany. *Received July 29, 1983*

ABSTRACT: The solution properties of poly(diacetylenes) [=(R)C—C≡C—C(R)]= were studied by using PTS-12 (R = $(CH_2)_4OSO_2C_6H_4CH_3$) and P3BCMU (R = $(CH_2)_3OCONHCH_2CO_2C_4H_9$) as the prime examples. The UV–vis, the resonance-Raman, and the ^{13}C-NMR spectra of the dissolved polymers may be interpreted by comparison with low molecular weight polyconjugated model substances as if the backbone skeleton consisted of segments of effective conjugation length n_{eff} decoupled from the other segments electronically by bond rotation. All three methods give the same value of n_{eff} of approximately 5–7 constitutive units. Light scattering and viscosity studies indicate, however, that the poly(diacetylenes) behave like a wormlike (Porod–Kratky) chain. The persistence length was determined for PTS-12 as 15–20 nm, corresponding to 30–40 constitutive units. In the framework of this model the backbone skeleton is continuously deformed down to the scale of the individual bonds. Thus, n_{eff} is recognized as being simply a number determined by using a calibration curve obtained from low molecular weight compounds, which are not necessarily models for the polymer. The blue-to-yellow transition observed to occur in solutions of P3BCMU was reinvestigated. In the yellow solutions P3BCMU exists molecularly dispersed in the form of a wormlike coil. The transition to the blue form, which is obtained by changing the temperature or solvent quality, was demonstrated to be an aggregation phenomenon and not a transition occurring within a single molecule (nonplanar-to-planar transition).

1. Introduction

Poly(diacetylenes) (PDA) (1) are unique among the synthetic organic polymers insofar as they can be obtained as perfect macroscopic single crystals by solid-state polymerization of suitably substituted diacetylenes (2).[1-7] The backbone of the PDA consists of conjugated double and triple bonds with the substituents R in all-trans-position with regard to the double bonds.

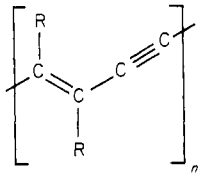

1

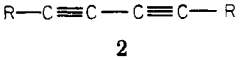

2

The conjugated backbone is the origin of the deep red to purple color and metallic luster of the polymer single crystals. The chain structure has been rigorously established by X-ray analyses in a large number of cases differing by the chemical nature of R[3,6-10] so that there does not remain any doubt that 1 gives the general and proper formulation of the bond sequence in PDAs. As expected, all the carbon atoms of the backbone are situated in a plane within the lattice and the chains are extended along a unique crystallographic axis, giving rise to an extremely anisotropic behavior of the PDA crystals concerning their mechanical, optical, and electrical properties. The field of PDA crystals, including the mechanism of solid-state polymerization,[11-14] has found widespread interest in recent years, and a number of reviews are available.[3,6,7,15] Very little is known, however, about the solution properties of PDA, owing to the extreme insolubility of most of the better investigated crystalline representatives of this class of polymers. Viscosity measurements and data on the solution spectra of some PDAs have been mentioned in the early reports on the solid-state polymerization of diacetylenes.[1,2,16] Since Patel et al. detected in 1978 that poly[4,6-decadiyne-1,10-diol bis((*n*-butoxycarbonyl)-methyl)urethane] (P3BCMU) (3) is a readily soluble polymer, the study of the solution properties of PDA chains[17-19] has attracted increasing interest. More recently, a fair number of soluble PDAs have been synthesized in our laboratory[20,21] and independently by Schulz and coworkers.[22,23] Some of the prominent representatives are mentioned in Table I. The most remarkable feature of these compounds is the dramatic blue shift of the optical absorption which is observed when the polymer crystals are dissolved. Typically, the crystals exhibit absorption spectra with a maximum around 600 nm, which shifts to approximately 450 nm on dissolution. Reprecipitation with concurrent recrystallization does not reconstitute the or-

† Dedicated to Professor Walter H. Stockmayer on the occasion of his 70th birthday with the warmest personal wishes.

0024-9297/84/2217-0837$01.50/0